amount of DNA (per weight) as brain tissue. However, plant DNA hybridizes to neither the human mtDNA probe nor a human *Alu* sequence probe.

The mtDNA digested poorly with restriction enzymes, as shown by the *Eco*RI digest (Figure 4*b*, lane 1), which does not exhibit the expected hybridizing 8-kb mtDNA fragment[6]. However, a significant conversion of open circular to linear molecules did take place, as expected if only a fraction of the *Eco*RI recognition sequences remained. Resistance to enzyme digestion is an intrinsic property of the old DNA as a bacterial plasmid DNA, mixed with an old DNA sample, was digested to completion. Similarly, old nuclear DNA was not easily digested, as similar blots probed with radiolabelled DNA and RNA representing nuclear sequences known to be present in multiple copies in the human genome, including an *Alu* sequence[7] and the large and small ribosomal RNAs[8] gave diffuse hybridization patterns, not distinct bands. This inability to digest the DNA completely is likely to be due to base modifications or other DNA damage leading to a loss of restriction enzyme site recognition. Preliminary results suggest that alkali-sensitive cleavage sites are present every few hundred base pairs (bp) in the old DNA, and we believe DNA damage is probably affecting both DNA digestion and hybridization efficiencies. DNA damage may also explain the presence of open circular mtDNA since inter-strand crosslinks, often formed after depurination in solution[9], will stabilize circular forms even in the presence of multiple single-strand breaks.

An independent estimate of the fraction of human DNA sequences in the old DNA samples is given by the quantification of *Alu* sequences in dot blots (data not shown). We estimate that *Alu* sequences are present at 1% of the level seen in an equivalent amount of human placental DNA, again suggesting either co-isolation of plant DNA with human sequences or sufficient DNA damage to reduce hybridization efficiency. At present, we cannot exclude either possibility.

This brain tissue dates from the Early Archaic period[16] (~8,000 yr ago) and is thus the oldest human soft tissue yet analysed at a molecular level. We have demonstrated the presence of human DNA and remnant cellular and anatomical structure in the tissue. It is especially noteworthy that this material has been preserved in an aqueous environment, suggesting that intact DNA can survive in other than extremely arid conditions, which greatly widens the sites where ancient genetic material may be found. We are now attempting to clone identifiable human genes or gene fragments.

We thank Windover Farms, Inc. and Jim Swann for their initial observation of the site, and for cooperation and financial support. This research was also supported by funds from the State of Florida. We thank Drs H. Baer, W. Buhi, S. Khan, R. Roberts, K. Scott, P. Small and S. Tanhauser, also L. Ballinger, K. Dodge, K. Dukes, C. Fletcher, W. Gage, P. Mitchell, L. Peters and T. Stone for helpful comments and technical assistance.

Received 20 March; accepted 19 August 1986.

1. Pääbo, S. *Nature* **314**, 644-645 (1985).
2. Higuchi, R., Bowman, B., Friedberger, M., Ryder, O. A. & Wilson, A. C. *Nature* **312**, 282-284 (1984).
3. Taubold, R. D. *et al. Lipids* **10**, 383-390 (1975).
4. Adams, R. D. & Lee, J. C. in *Histology and Histopathy of the Nervous System* (eds Haymaker, W. & Adams, R. D.) 234-237 (Thomas, Springfield, 1982).
5. Chang, D. D. & Clayton, D. A. *Proc. natn. Acad. Sci. U.S.A.* **82**, 351-355 (1985).
6. Anderson, S. *et al. Nature* **296**, 457-465 (1981).
7. Houck, C. M., Rinehart, F. P. & Schmid, C. W. *J. molec. Biol.* **132**, 289-306 (1979).
8. Long, E. O. & Dawid, I. B. *A. Rev. Biochem.* **49**, 727-764 (1980).
9. Goffin, C., Bricteux-Grégoire, S. & Verly, W. G. *Biochim. biophys. Acta* **783**, 1-5 (1984).
10. Klein, H., Lerman, J., Damon, P. & Ralph, E. *Radiocarbon* **24**, 103-150 (1982).
11. Luna, L. G. *Manual of Histological Staining Methods of the Armed Forces Institute of Pathology* 3rd edn (McGraw-Hill, New York, 1968).
12. Anderson, S. *et al.* in *Mitochondrial Genes* (eds Slonimisky, P., Borst, P. & Attardi, G.) 5-43 (Cold Spring Harbor Laboratory, New York, 1982).
13. Hixson, J. A. thesis, Univ. Michigan (1983).
14. Upholt, W. B. & Dawid, I. B. *Cell* **11**, 571-583 (1977).
15. Brown, W. W., George, M. Jr & Wilson, A. C. *Proc. natn. Acad. Sci. U.S.A.* **76**, 1967-1971 (1979).
16. Mitanich, J. T. & Charles, C. H. *Fairbank Florida Archaeology* **23** (Academic, New York, 1980).

Mapping human visual cortex with positron emission tomography

Peter T. Fox*†, Mark A. Mintun*, Marcus E. Raichle*‡, Francis M. Miezin§, John M. Allman§ & David C. Van Essen§

* Department of Radiology, † Department of Neurology and Neurological Surgery (Neurology) and ‡ McDonnell Center for Studies of Higher Brain Function, Washington University School of Medicine, St Louis, Missouri 63110, USA
§ Division of Biology, California Institute of Technology, Pasadena, California 91125, USA

Positron-emission tomography (PET) can localize functions of the human brain by imaging regional cerebral blood flow (CBF) during voluntary behaviour. Functional brain mapping with PET, however, has been hindered by PET's poor spatial resolution (typically >1 cm). We have developed an image-analysis strategy that can map functional zones not resolved by conventional PET images. Brain areas selectively activated by a behavioural task can be isolated by subtracting a paired control-state image from the task-state image, thereby removing areas not recruited by the task. When imaged in isolation the centre of an activated area can be located very precisely. This allows subtle shifts in response locale due to changes in task to be detected readily despite poor spatial resolution. As an initial application of this strategy we mapped the retinal projection topography of human primary visual cortex. Functional zones separated by less than 3 mm (centre-to-centre) were differentiated using PET CBF images with a spatial resolution of 18 mm. This technique is not limited to a particular brain area or type of behaviour but does require that the increase in CBF produced by the task be both intense and focal.

PET records the spatial distribution of an administered radionuclide in selected planes of the *in vivo* brain. Spatial resolution in PET images, however, is inherently limited. This limitation is described most simply by reference to point sources of radioactivity, as follows. Emission detection and image reconstruction blur a point source into an activity distribution or point-spread function[1] (Fig. 1). As two simultaneously imaged point sources cannot be discriminated when they lie closer together than the width of one point-spread function at its half-maximum amplitude (the full-width at half-maximum or FWHM), this is the usual measure of spatial resolution for PET (Fig. 1). The spatial resolution of most PET images is greater than 1.0 cm (FWHM).

A distinction can be drawn, however, between spatial resolution and source localization. Two adjacent point sources cannot be resolved when separated by less than one FWHM. A single point source, however, can be localized with a precision well below the FWHM (Fig. 1). This phenomenon is well known in signal detection theory[2] and has been postulated to underlie the property of hyperacuity in the human visual system[3]. In application to PET, this suggests that zones of brain activity separated by less than one FWHM could be distinguished from one another by sequential activation even though they would not be seen as distinct (not resolved) if activated simultaneously (Fig. 1).

Local alterations in neuronal electrical activity occur during task performance (such as stimulation) and induce local changes in CBF[4]. As CBF in nonactivated brain areas is quite stable over time[5], a resting-state CBF image can be directly subtracted from a stimulated-state image to create a new image showing only the focal changes in CBF caused by the activation task. In subtraction format, a local CBF change appears as an isolated focus of high activity within a low-level background, quite similar to the image of an isolated point source. This provides a means for applying the principle described above. Brain areas lying closer together than one FWHM should be discriminable by activating each area in isolation and determining the location

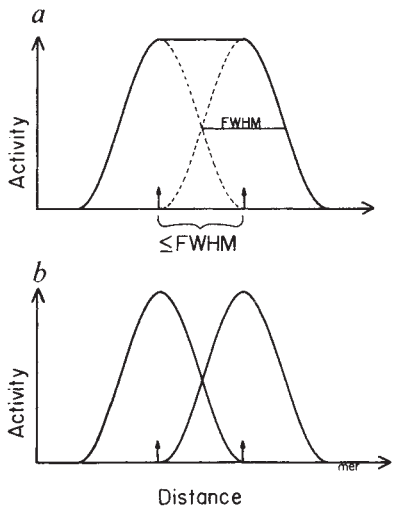

Fig. 1 Due to the limited spatial resolution of emission imaging, a point source of radioactivity is imaged as an activity distribution (point-spread function) composed of a central maximum surrounded by a radially declining skirt of activity. Spatial resolution traditionally has been defined by the width of the point-spread function at half-peak activity (full-width at half-maximum or FWHM). *a*, Two simultaneously imaged point sources cannot be resolved when separated by a distance of one FWHM or less. *b*, Isolated point sources localized with a precision well below the FWHM, allow sequentially imaged sources with a centre-to-centre separation much less than the FWHM to be distinguished by a difference in the location of the centres of the activity distributions.

of each response within subtraction-format images. As an initial application of this experimental strategy, we mapped the representation of the central retina in human primary visual cortex.

Test stimuli were checkerboard rings about a central fixation point (Fig. 2). Three eccentricities were tested: macular (0.1–1.5°), perimacular (1.5–5.5°) and peripheral (5.5–15.5°). The control stimulus was a fixation point only. Stimulus presentation began 30–40 s before scan initiation and continued throughout

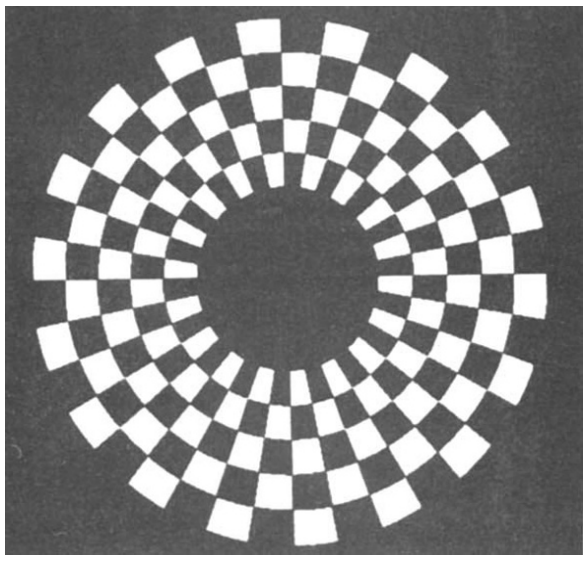

Fig. 2 All visual stimuli were checkerboard annuli with a central fixation point. The peripheral stimulus is shown and extended from 5.5 to 15.5°. The perimacular annulus extended from 1.5 to 5.5°. The macular annulus extended from 0.1 to 1.5°. Check size increased with eccentricity from 0.5 to 2.0°. Checks were red on black and alternated colours at 10 Hz to maximize the induced CBF response[5].

scan acquisition. Seventeen test-control pairs of CBF scans were obtained from six normal volunteers: five macular, six perimacular, six peripheral.

Water labelled with oxygen-15 ($H_2{}^{15}O$), a positron-emitting radiotracer with a half-life of 123 s, was used to measure brain blood flow. This tracer was given as a bolus injection into a peripheral vein and circulated into the brain within 10–20 s. A 40-s scan recorded the distribution of the administered radioactivity within the brain, from which images of regional CBF (Fig. 3*a*) were calculated[6,7]. A 10-min interscan interval was sufficient for isotope decay (five half-lives) and to reestablish resting levels of regional CBF within activated areas[5]. Images of regional CBF change (Fig. 3*b,c,d*) were formed by paired subtraction of control-state from stimulated-state CBF measurements[8]. Response foci were located by computer algorithm and plotted in stereotactic coordinates (Table 1)[9].

Response locale varied systematically with stimulus field (Table 1). Macular responses were posterior and inferior, lying at the occipital pole (Fig. 3*b*). Peripheral responses were anterior and superior, lying on the medial occipital surface (Fig. 3*d*). Perimacular responses lay between macular and peripheral (Fig. 3*c*). Shifts in cortical response locale as small as 3 mm were readily detected and statistically significant (Table 1).

The cortical magnification factor, defined as the linear extent of striate cortex to which each degree of the retinal field projects[10–12], was calculated for three retinal eccentricities (Table 2) from the observed response locations (Table 1). As cortical

Table 1 Response locale in stereotactic coordinates

Stimulus field	Macula	Perimacula	Periphery
Degrees	0.1–1.5	1.5–5.5	5.5–15.5
n	5	6	6
Antero-posterior axis (cm)			
Mean (s.d.)	−6.86 (0.13)	−6.29 (0.09)	−5.96 (0.07)
Statistical analysis	ANOVA: $F=42$, $P<0.0001$		
	Newman-Keuls:		
	Macula < perimacula < periphery,		
	$P<0.01$ for all inequalities		
Vertical axis (cm)			
Mean (s.d.)	−0.50 (0.36)	−0.12 (0.32)	−0.64 (0.42)
Statistical analysis	ANOVA: $F=90$, $P<0.00001$		
	Newman-Keuls:		
	Macula < perimacula < periphery		
	$P<0.01$ for all inequalities		

Degrees indicates the inner and outer boundaries of an annular stimulus in degrees of eccentricity from the fixation point. Response foci were located by a three-dimensional search for the centre of the maximum response (peak CBF change) using a roving cubic (7.0 cm^3) region of interest and a centre-of-mass algorithm. All responses lay in the midsagittal plane. As significant shifts in response locale occurred only along the antero-posterior and vertical axes, only these dimensions are reported. Distances are in cm from the centre of the AC–PC line in proportionately measured stereotactic coordinates[9].

infolding and curvature of the calcarine fissure were not visualized, these values set a lower boundary rather than a mean.

Our observations confirm and extend prior studies of human visual cortex. Case reports of patients with occipital lobe lesions established the general outline of retinal:cortical projection topography, but lacked accurate descriptions of lesion locale and were limited by the stereotypy of spontaneous lesions[13–16]. Plots of the perceived location of visual illusions (phosphenes) induced by electrical stimulations of the occipital cortex during neurological surgery have been reported, but gave irregular and discontinuous maps[17,18]. Evoked magnetic field recordings have detected field-source shifts in response to shifts in stimulus eccentricity, but could not specify unequivocally the anatomical sites of the fields' sources and needed rather gross stimuli to evoke measurable fields[19]. The PET imaging strategy presented

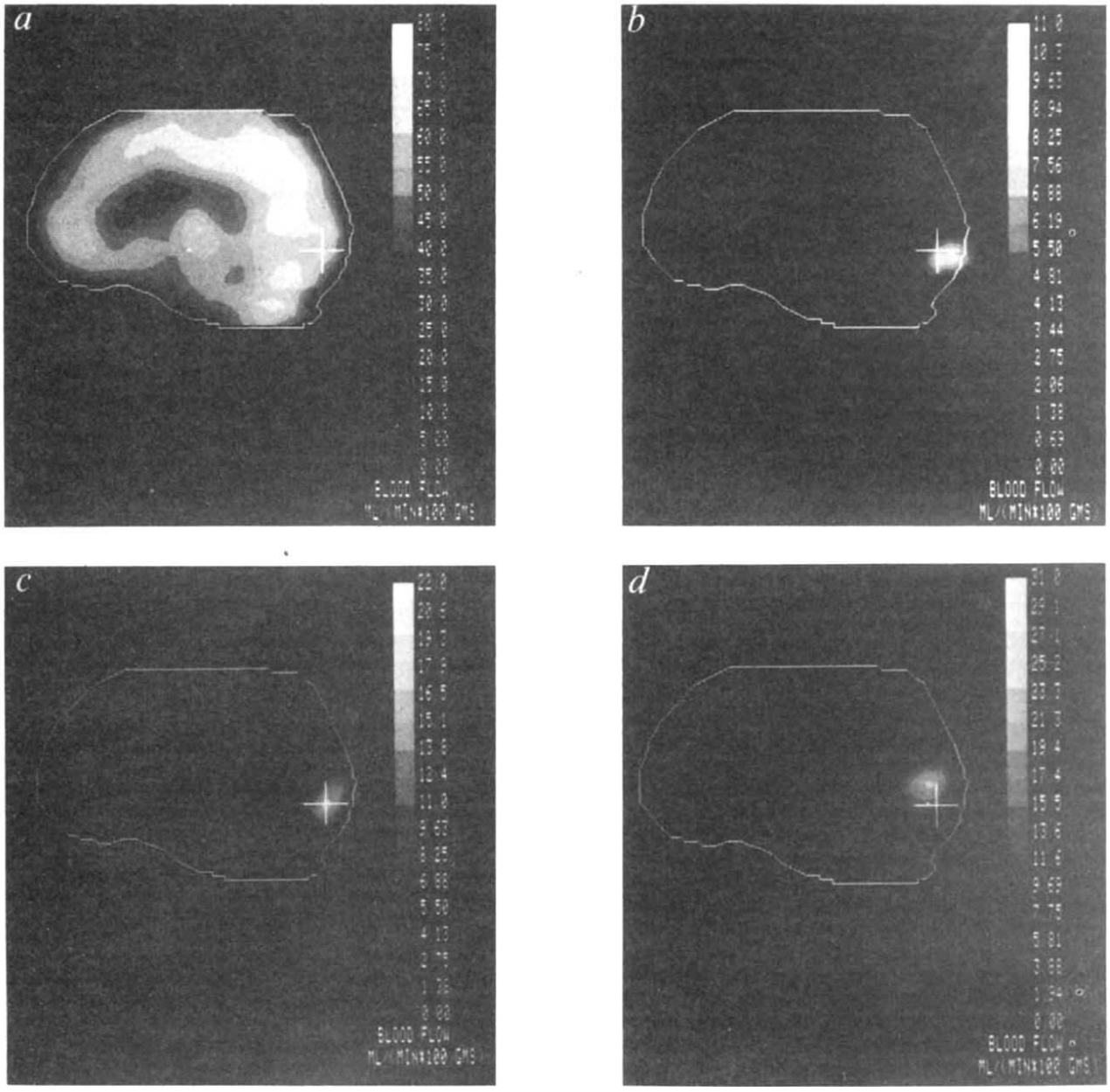

Fig. 3 All images are midsagittal sections formed by summing the images of all six subjects within a standardized stereotactic coordinate space[9]. Anterior is to the left. The brain boundary was obtained from image A and is positioned identically in all four images. The horizontal fiducial lies on the line connecting the anterior and posterior commissures (bicommissural or AC-PC line[9]). The vertical fiducial lies 6.2 cm posterior to the centre of the bicommissural line. Both fiducials are 2.0 cm long. Units of blood flow are ml g^{-1} min^{-1}. *a*, Resting-state image of cerebral blood flow (CBF). *b*, Macular response focus (0.1–1.5° stimulus) in a subtraction image format. The response lies most posterior and inferior, at the occipital pole. *c*, Perimacular response focus (1.5–5.5° stimulus) in subtraction image format, intermediate in location between the macular and peripheral responses. *d*, Peripheral response focus (5.5–15.5° stimulus) in subtraction image format, lying anterior and superior to the two other responses.

here yielded an orderly, continuous, retinotopic map in agreement with the order of retinal projections to visual cortex observed in non-human primates[20,21] and expected by homology in man. The anatomical precision of this map exceeds those previously attained in man. These observations also have provided the first direct, non-invasive measurements of cortical magnification factor in humans.

Computer simulations (to be reported separately) were performed to define further the properties of this imaging strategy. Three findings bear mention. First, the accuracy with which a focal CBF change is localized increases with the intensity of the CBF response. Second, localization accuracy of 0.5–1.5 mm can be attained with an image resolution of 18 mm (FWHM) and focal CBF change of only 20–30% (comparable to those observed in this study). Finally, the effective spatial resolution achieved with this technique should increase with the spatial resolution (FWHM) of the tomograph employed. As PET instrumentation evolves, therefore, the precision achieved with this mapping strategy should continue to improve.

Applications of this strategy for high-resolution functional brain mapping potentially are quite broad. In principle, any brain region undergoing increased neuronal work and, thereby, increased regional CBF during task performance can be mapped. Mapping precision, however, will vary with the intensity and focality of the task's induced CBF change, both of which will be strongly affected by task design[4,5,8]. Our pilot application of this technique mapped primary visual cortex. Similar studies of primary somatosensory and auditory cortices

Table 2 Magnification factor in human striate cortex

Comparison	Macula to perimacula	Macula to periphery	Perimacula to periphery
Response shift (mm)	9.4	15.6	6.6
Stimulus shift (degrees)	2.8	9.8	7.0
Mean eccentricity (degrees)	2.1	5.6	7.0
Magnification factor (mm per degree)	3.4	1.6	0.9

These values were calculated from the mean eccentricity of each stimulus pattern (macula = 0.7°, perimacula = 3.5°, periphery = 10.5°) and the mean response locale for each stimulus locale as given in Table 1. Degrees indicate degrees of eccentricity from the fixation point. Magnification factors are expressed in millimetres of striate cortex per degree of eccentricity of retinal visual field[10–12].

and higher-order cortical zones are under way. Detailed mapping of brain areas participating in such uniquely human activities as language, cognition and emotion should follow in due course and hold still greater interest and potential.

Received 10 January; accepted 11 August 1986.

1. Yamamoto, M., Ficke, D. C. & Ter-Pogossian, M. M. *IEEE Trans. nucl. Sci.* **29**, 529–533 (1982).
2. Lahti, B. P. *Signals, Systems, and Communication*, 437–441 (New York, 1965).
3. Westheimer, G. *Invest. ophthal. vis. Sci.* **18**, 893–912 (1979).
4. Fox, P. T. & Raichle, M. E. *Proc. natn. Acad. Sci. U.S.A.* **83**, 1140–1144 (1986).
5. Fox, P. T. & Raichle, M. E. *J. Neurophysiol.* **51**, 1109–1120 (1984).
6. Herscovitch, P., Markham, J & Raichle, M. E. *J. nucl. Med.* **24**, 782–789 (1983).
7. Raichle, M. E., Martin, W. R. W., Herscovitch, P., Mintun, M. A. & Markham, J. *J. nucl. Med.* **24**, 790–798 (1983).
8. Fox, P. T., Fox, J. M., Raichle, M. E. & Burde, R. M. *J. Neurophysiol.* **54**, 348–369 (1985).
9. Fox, P. T., Perlmutter, J. S. & Raichle, M. E. *J. Comput. Assist. Tomogr.* **9**, 141–153 (1985).
10. Daniel, P. M. & Whitteridge, D. *J. Physiol., Lond.* **159**, 203–221 (1961).
11. Cowey, A. & Rolls, E. T. *Expl Brain Res.* **21**, 447–454 (1974).
12. Rovamo, J. & Virsu, V. *Expl Brain Res.* **37**, 495–510 (1979).
13. Holmes, G. *Br. J. Ophthal.* **2**, 353–384 (1918).
14. Spalding, J. M. D. *J. Neurol. Neurosurg. Psychiat.* **15**, 169–183 (1952).
15. Teuber, H., Battersby, W. & Bender, M. *Visual Field Deficits after Penetrating Missile Wounds* (Harvard University Press, Cambridge, 1960).
16. McAuley, D. L. & Ross-Russell, R. W. *J. Neurol. Neurosurg. Psychiat.* **42**, 298–311 (1979).
17. Brindley, G. S. in *Handbook of Sensory Physiology* 7 (3B) (ed. Jung, R.) 583–594 (Springer, Berlin, 1973).
18. Dobelle, W. H., & Mladejovsky, M. G. *J. Physiol., Lond.* **243**, 553–576 (1974).
19. Maclin, E., Okada, Y. C., Kaufman, L. & Williamson, S. J. *Nuov. Cim.* **2**, 410–419 (1983).
20. Van Essen, D. C., Newsome, W. T. & Maunsell, J. H. R. *Vision Res.* **24**, 429–448 (1984).
21. Talbot, S. A. & Marshall, W. H. *Am. J. Ophthal.* **24**, 1255 (1941).

Calcitonin gene-related peptide regulates muscle acetylcholine receptor synthesis

Helen V. New & Anne W. Mudge

MRC Neuroimmunology Programme, Department of Zoology, University College London, Gower Street, London WC1E 6BT, UK

Innervation of muscle by motoneurones induces the development of a characteristic, high density cluster of acetylcholine receptors (AChRs) at the neuromuscular junction[1–4]. Studies *in vitro* show that the accumulation of AChRs at nerve–muscle contacts results from both increased insertion of new AChRs into the muscle plasma membrane beneath nerve terminals[5] and redistribution of pre-existing AChRs[5–7]; these two modes of AChR accumulation may be separately controlled since factors have been identified that influence AChR redistribution but not synthesis[8,9]. Although many aspects of muscle development are regulated by nerve-dependent muscle activity[10–16], junctional AChR clusters still develop when neuromuscular transmission is blocked by either curare or α-bungarotoxin[1,5,6,17], suggesting that their formation is mediated by nerve-derived trophic factors other than activity. A molecule immunologically related to calcitonin gene-related peptide (CGRP-I) has been found in motoneurones in a variety of mammals including man[18,19]. Here we provide indirect evidence that CGRP-I may be a motoneurone-derived trophic factor that increases AChR synthesis at vertebrate neuromuscular junctions.

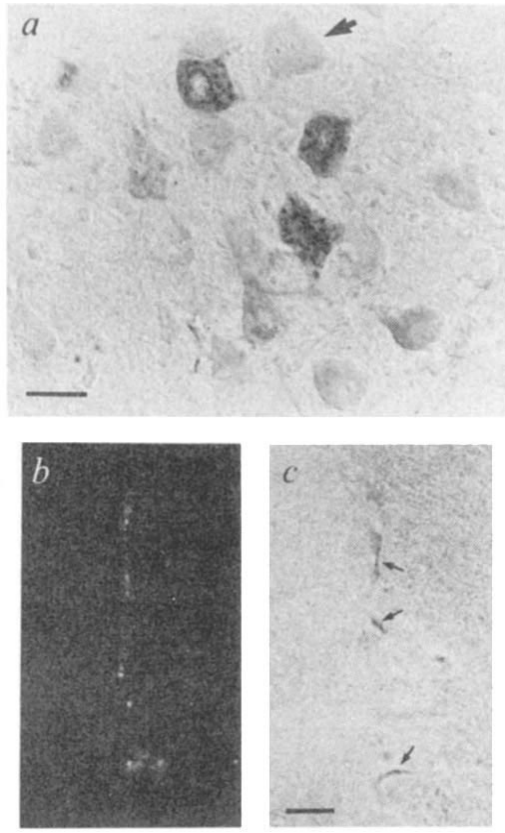

Fig. 1 Immunohistochemical localization of CGRP-I in embryonic chick motoneurones. *a*, Granular CGRP immunoreactivity in a subpopulation of motoneurone cell bodies at E17. The arrow points to an unstained motoneurone. Bar = 30 μm. *b*, CGRP immunoreactivity in a section of E14 leg muscle. *c*, AChE staining of the same field as in *b*. Arrows point to neuromuscular junctions. Bar = 10 μm.

Methods. Cryostat sections of tissue fixed in 4% paraformaldehyde (pfa) were processed for staining by the peroxidase anti-peroxidase method using 3,3′-diaminobenzidine tetrahydrochloride (Polysciences) as described previously[22]. Rabbit antiserum to CGRP (Cambridge Research Biochemicals; lot CGR-37) was used at 1:400. Staining was abolished in control serial sections incubated with antiserum together with 10^{-7} M CGRP (Sigma). For double-labelling of sections with AChE and CGRP, sections were first stained for AChE[34], washed and then incubated with anti-CGRP antibody overnight at 4 °C. The second antibody was sheep anti-rabbit-immunoglobulin conjugated to fluorescein isothiocyanate (Wellcome), at 1:100. Sections mounted in glycerol with DABCO[35]; viewed with a Zeiss microscope equipped with either epifluorescence (*b*) or differential interference contrast optics (*c*).

A rabbit antiserum to CGRP was used to stain cryostat sections from the lumbosacral region of developing chicks by the peroxidase anti-peroxidase method. Many large cells in the ventral horn of the spinal cord showed granular cytoplasmic staining (Fig. 1*a*); from their size and position in the lateral motor column (LMC) these cells were identified as motoneurones. CGRP-I was present in a few cells of the chick lumbosacral LMC at embryonic day 6 (E6), and was in approximately half the motoneurones throughout the rostrocaudal axis from E7.5 onward. Although a subpopulation of motoneurones was strongly CGRP-immunoreactive throughout development,